Variation of guest selectivity within [Fe$_4$L$_4$]$^{8+}$ tetrahedral cages through subtle modification of the face-capping ligand.

Alan Ferguson*, Robert W. Staniland, Christopher M. Fitchett, Marie A. Squire, Bryce E. Williamson, and Paul E. Kruger*

MacDiarmid Institute for Advanced Materials and Nanotechnology, Department of Chemistry, University of Canterbury, Private Bag 4800, Christchurch 8140, New Zealand. E-mail: paul.kruger@canterbury.ac.nz

Electronic Supporting Information (ESI)

Materials and Methods

All reagents were used as received without further purification from BDH and Sigma Aldrich.

2,4,6-tris(4-aminophenoxy)triazine and 1,3,5-tris(4-aminophenoxy)benzene were prepared according to literature procedures.[S1, S2]

^{1}H and ^{19}F NMR spectroscopy was carried on an Agilent 400 NMR spectrometer operating at 400 MHz for ^{1}H and 376 MHz for ^{19}F. Chemical shifts are described in parts per million (ppm) on the δ scale.

High resolution mass spectra were recorded with a Bruker maXis 3G UHR-TOF mass spectrometer.

Infrared spectra were recorded on a Perkin Elmer Spectrum One FTIR spectrometer in the range 400-4000 cm^{-1}. Samples were analysed *via* diffuse reflectance in ground KBr.

General synthesis of [Fe₄L1₄]⁸⁺ (1).

25 mg of 2,4,6-tris(4-aminophenoxy)triazine (0.063 mmol) was dissolved in 10 mL of CH_3CN. To this solution 1.80 mL (0.189 mmol) of a 2-pyridinecarboxaldehyde-MeCN stock solution (1:100) was added with stirring. Solid $Fe(A^-)_2$ (0.063 mmol) ($A^- = BF_4^-$; OTf^-; PF_6^-; or ClO_4^-) was added, producing deep purple solutions, which were heated at ~50 °C overnight. ^1H and ^{19}F NMR samples were prepared by taking small portions of the reaction mixtures, removing the solvent, and then dissolving the residues in CD_3CN. Crystals suitable for X-ray diffraction were obtained by vapour diffusion of diisopropyl ether into the reaction mixture of the BF_4^- and OTf^- derivatives.
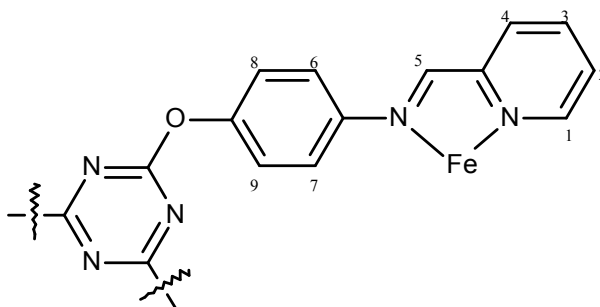
$[BF_4^-\subset 1]^{7+}[BF_4^-]_7$: ^1H NMR (400 MHz, CD_3CN): 5.08 (d, $J = 7.8$ Hz, 1 H, H7), 5.78 (d, $J = 6.8$ Hz, 1 H, H6), 7.13 (d, $J = 6.8$ Hz, 1 H, H8), 7.31 (d, $J = 4.7$ Hz, 1 H, H4), 7.36 (d, $J = 7.8$ Hz, 1 H, H9), 7.75 (t, $J = 6.0$ Hz, 1 H, H3), 8.38 (t, $J = 7.4$ Hz, 1 H, H2), 8.54 (d, $J = 7.4$ Hz, 1 H, H1), 8.83 (s, 1 H, H5); ^{19}F NMR (376 MHz, CD_3CN) -160.6 (s, 1 F), -151.8 (s, 7 F); m/z (HR-ESI-MS): 426.9483 $[BF_4^- + Fe_4L1_4]^{7+}$, $\overline{V}_{max}/cm^{-1}$ (KBr): 3624, 3544, 3165, 3004, 2945, 1633, 1575, 1219, 1196, 1039, 918, 750.

$[OTf^-\subset 1]^{7+}[OTf^-]_7$: ^1H NMR (400 MHz, CD_3CN): 5.21 (d, $J = 7.4$ Hz, 1 H, H7), 5.82 (d, $J = 7.2$ Hz, 1 H, H6), 7.18 (d, $J = 7.2$ Hz, 1 H, H8), 7.31 (d, $J = 3.9$ Hz, 1 H, H4), 7.45 (d, $J = 7.4$ Hz, 1 H, H9), 7.75 (t, $J = 6.3$ Hz, 1 H, H3), 8.37 (t, $J = 7.8$ Hz, 1 H, H2), 8.54 (d, $J = 7.4$ Hz, 1 H, H1), 8.84 (s, 1 H, H5); ^{19}F NMR (376 MHz, CD_3CN): -79.3 (s, 7 F), -77.7 (s, 1 F); m/z (HR-ESI-MS): 435.7960 $[OTf^- + Fe_4L1_4]^{7+}$, 533.2548 $[(OTf^-)_2 + Fe_4L1_4]^{6+}$, 669.8959 $[(OTf^-)_3 + Fe_4L1_4]^{5+}$, 874.6081 $[(OTf^-)_4 + Fe_4L1_4]^{4+}$; $\overline{V}_{max}/cm^{-1}$ (KBr): 3619, 3544, 3165, 3004, 2944, 1631, 1575, 1273, 1219, 1195, 1157, 1039, 918, 750.

$[PF_6^-\subset 1]^{7+}[PF_6^-]_7$: ^1H NMR (400 MHz, CD_3CN): 5.09 (d, $J = 7.8$ Hz, 1 H, H7), 5.79 (d, $J = 6.8$ Hz, 1 H, H6), 7.14 (d, $J = 6.8$ Hz, 1 H, H8), 7.31 (d, $J = 5.5$ Hz, 1 H, H4), 7.37 (d, $J = 7.8$ Hz H, H9), 7.75 (t, $J = 6.7$ Hz, 1 H, H3), 8.38 (t, $J = 7.4$ Hz, 1 H, H2), 8.53 (d, $J = 7.0$ Hz, 1 H, H1), 8.83 (s, 1 H, H5); ^{19}F NMR (376 MHz, CD_3CN): -75.2 (s, 1 F), -73.9 (s, 7 F), -73.3 (s, 1 F), -72.0 (s, 7 F); m/z (HR-ESI-MS): 435.2274 $[PF_6^- + Fe_4L1_4]^{7+}$, 667.3043 $[(PF_6^-)_3 + Fe_4L1_4]^{5+}$, 870.3705 $[(PF_6^-)_4 + Fe_4L1_4]^{4+}$; $\overline{V}_{max}/cm^{-1}$ (KBr): 3623, 3540, 3164, 3004, 2944, 1631, 1574, 1218, 1195, 1039, 918, 847, 749.

$[ClO_4^-\subset 1]^{7+}[ClO_4^-]_7$: ^1H NMR (400 MHz, CD_3CN): 5.08 (d, $J = 7.4$ Hz, 1 H, H7), 5.78 (d, $J = 7.8$ Hz, 1 H, H6), 7.14 (d, $J = 7.8$ Hz, 1 H, H8), 7.32 (d, $J = 5.1$ Hz, 1 H, H4), 7.38 (d, $J = 7.4$ Hz, 1 H, H9), 7.75 (t, $J = 6.0$ Hz, 1 H, H3), 8.38 (t, $J = 7.0$ Hz, 1 H, H2), 8.54 (d, $J = 7.0$ Hz, 1 H, H1), 8.83 (s, 1 H, H5); m/z (HR-ESI-MS): 4328.7963 $[ClO_4^- + Fe_4L1_4]^{7+}$, 516.7550 $[(ClO_4^-)_2 + Fe_4L1_4]^{6+}$; $\overline{V}_{max}/cm^{-1}$ (KBr): 3621, 3543, 3165, 3004, 2945, 1631, 1574, 1219, 1196, 1035, 918, 750.

General synthesis of [Fe₄L2₄]⁸⁺ (2).

25 mg of 1,3,5-tris(4-aminophenoxy)benzene (0.062 mmol) was dissolved in 10 mL of CH_3CN. To this solution 1.76 mL (0.186 mmol) of a 2-pyridinecarboxaldehyde-MeCN stock solution (1:100) was added with stirring. Solid Fe(A⁻)₂ (0.062 mmol) (A⁻ = BF_4^-; OTf⁻; PF_6^-; ClO_4^-, or NTf_2^-) was added, producing deep purple solutions, which were heated at ~50 °C overnight. ¹H and ¹⁹F NMR samples were prepared by taking small portions of the reaction mixtures, removing the solvent, and then dissolving the residues in CD_3CN. Crystals suitable for X-ray diffraction were obtained by vapour diffusion of diethyl ether into the reaction mixture of the NTf⁻ derivative.
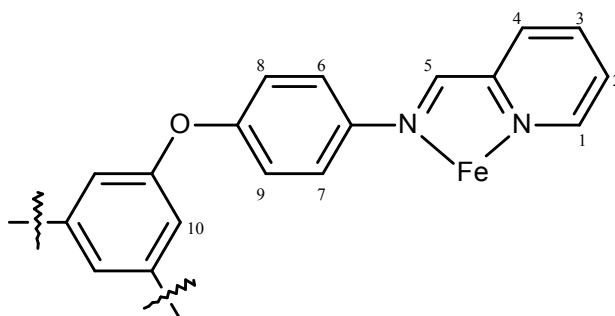
[2]⁸⁺[BF₄⁻]₈: ¹H NMR (400 MHz, CD_3CN): 5.33 (brs, 1 H, H7), 5.86 (brs, 1 H, H6), 6.23 (s, 1 H, H10), 6.85 (brs, 1 H, H8), 7.25 (brs, 1 H, H9), 7.39 (d, J = 5.1 Hz, 1 H, H4), 7.78 (t, J = 6.1 Hz, 1 H, H3), 8.41 (t, J = 7.6 Hz, 1 H, H2), 8.54 (d, J = 7.4 Hz, 1 H, H1), 8.94 (s, 1 H, H5); ¹⁹F NMR (376 MHz, CD_3CN): -151.1; m/z (HR-ESI-MS): 361.2155 [Fe₄L1₄]⁸⁺; $\overline{V}_{max}$/cm⁻¹ (KBr): 3595, 2926, 1587, 1497, 1460, 1305, 1232, 1166, 1058, 1008, 862, 845, 774.

[OTf⊂2]⁷⁺[OTf⁻]₇: ¹H NMR (400 MHz, CD_3CN): 5.46 (d, J= 9.0 Hz, 1 H, H7), 5.60 (d, J = 8.6 Hz, 1 H, H6), 6.10 (s, 1 H, H10), 7.06 (d, J = 8.6 Hz, 1 H, H8), 7.39 (d, J = 5.1 Hz, 2 H, H4), 7.45 (d, J = 9.0 Hz, 1 H, H9), 7.75 (t, J = 6.6 Hz, 1 H, H3, 8.39 (t, J = 7.8 Hz, 1 H, H2), 8.48 (d, J = 7.8 Hz, 1 H, H1), 8.86 (s, 1 H, H5); ¹⁹F NMR (376 MHz, CD_3CN): -79.3 (s, 7 F), -78.6 (s, 1 F); m/z (HR-ESI-MS): 434.0909 [OTf⁻ + Fe₄L2₄]⁷⁺, 667.5082 [(OTf⁻)₃ + Fe₄L2₄]⁵⁺; 871.6251 [(OTf⁻)₄ + Fe₄L2₄]⁴⁺; $\overline{V}_{max}$/cm⁻¹ (KBr): 3621, 3542, 3164, 3003, 2944, 1627, 1586, 1272, 1226, 1157, 1039, 918, 745.

[PF₆⁻⊂2]⁷⁺[PF₆⁻]₇: ¹H NMR (400 MHz, CD_3CN): 5.41 (d, J= 8.2 Hz, 1 H, H7), 5.58 (d, J = 8.6 Hz, 1 H, H6), 6.07 (s, 1 H, H10), 7.06 (d, J = 8.6 Hz, 1 H, H8), 7.33 (d, J = 8.2 Hz, 2 H, H9), 7.40 (d, J = 5.1 Hz, 1 H, H4), 7.75 (t, J = 6.0 Hz, 1 H, H3), 8.39 (t, J = 7.6 Hz, 1 H, H2), 8.48 (d, J = 7.4 Hz, 1 H, H1), 8.85 (s, 1 H, H5) ¹⁹F NMR (376 MHz, CD_3CN): -76.0 (s, 1 F), -74.1 (s, 1 F), -73.6 (s, 9 F), -71.7 (s, 9 F); m/z (HR-ESI-MS): 433.5207 [PF₆⁻ + Fe₄L2₄]⁷⁺; 529.9352 [(PF₆⁻)₂ + Fe₄L2₄]⁶⁺; 664.9151 [(PF₆⁻)₃ + Fe₄L2₄]⁵⁺; 867.3844 [(PF₆⁻)₄ + Fe₄L2₄]⁴⁺; $\overline{V}_{max}$/cm⁻¹ (KBr): 3624, 3546, 3165, 3004, 2945, 1633, 1572, 1219, 1196, 1039, 918, 848, 750.

[2]⁸⁺[ClO₄⁻]₈: ¹H NMR (400 MHz, CD_3CN): 5.32 (brs, 1 H, H7), 5.87 (brs, 1 H, H6), 6.22 (s, 1 H, H10), 6.84 (brs, 1 H, H8), 7.24 (brs, 1 H, H9), 7.40 (d, J = 5.1 Hz, 1 H, H4), 7.77 (t, J = 6.5 Hz, 1 H, H3), 8.40 (t, J = 7.8 Hz, 1 H, H2), 8.51 (d, J = 7.8 Hz, 1 H, H1), 8.94 (s, 1 H, H5); m/z (HR-ESI-MS): 427.0911 [ClO₄⁻ + Fe₄L2₄]⁷⁺, 514.7654 [(ClO₄⁻)₂ + Fe₄L2₄]⁶⁺, 637.7074 [(ClO₄⁻)₃ + Fe₄L2₄]⁵⁺, 822.8697 [(ClO₄⁻)₄ + Fe₄L2₄]⁴⁺; $\overline{V}_{max}$/cm⁻¹ (KBr): 3628, 3037, 1588, 1495, 1452, 1303, 1225, 1165, 1095, 1007, 841, 772, 623.

[2]⁸⁺[NTf₂⁻]₈: ¹H NMR (400 MHz, CD_3CN): ¹H NMR (400 MHz, CD_3CN), 5.32 (brs, 1 H, H7), 5.87 (brs, 1 H, H6), 6.22 (s, 1 H, H10), 6.84 (brs, 1 H, H8), 7.24 (brs, 1 H, H9), 7.39 (d, J = 5.1 Hz, 1 H, H4), 7.78 (t, J = 6.4 Hz, 1 H, H3), 8.41 (t, J = 7.4 Hz, 1 H, H2), 8.53 (d, J = 7.4 Hz, 1 H, H1), 8.94 (s, 1 H, H5); ¹⁹F NMR (376 MHz, CD_3CN): -80.2; m/z (HR-ESI-MS): 575.0890 [(NTf⁻)₂ + Fe₄L2₄]⁶⁺, 746.0898 [(NTf⁻)₃ + Fe₄L2₄]⁵⁺, 1002.5891 [(NTf⁻)₄ + Fe₄L2₄]⁴⁺; $\overline{V}_{max}$/cm⁻¹ (KBr): 3038, 2456, 1590, 1497, 1459, 1347, 1198, 1135, 1058, 1007, 863, 768, 740, 613, 570, 513.

Summary of ^{1}H and ^{19}F NMR data for $[Fe_4L1_4]^{8+}$ (1) and $[Fe_4L2_4]^{8+}$ (2) complexes.
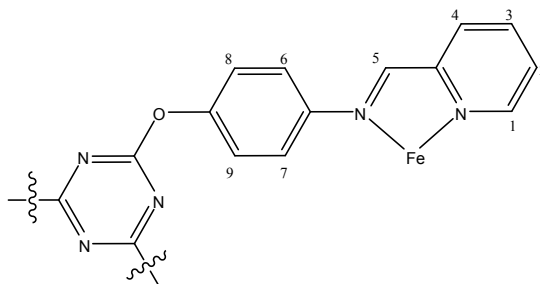
^{1}H NMR data for 1 (significant shifts *cf.* other anions highlighted: <mark>upfield</mark>, <mark>downfield</mark>)

	$[BF_4^-{\subset}1](BF_4^-)_7$	$[OTf^-{\subset}1](OTf^-)_7$	$[PF_6^-{\subset}1](PF_6^-)_7$	$[ClO_4^-{\subset}1](ClO_4^-)_7$
H7	5.08	5.21	5.09	5.08
H6	5.78	5.82	5.79	5.78
H8	7.13	7.18	7.14	7.14
H4	7.31	7.31	7.31	7.32
H9	7.36	7.45	7.37	7.38
H3	7.75	7.75	7.75	7.75
H2	8.38	8.37	8.38	8.38
H1	8.54	8.54	8.53	8.54
H5	8.83	8.84	8.83	8.83

^{19}F NMR data for 1

$[BF_4^-{\subset}1](BF_4^-)_7$:	-160.6 (s, 1 F, *endo*) -151.8 (s, 7 F, *exo*);
$[OTf^-{\subset}1](OTf^-)_7$:	-79.3 (s, 7 F, *exo*) -77.7 (s, 1 F, *endo*);
$[PF_6^-{\subset}1](PF_6^-)_7$:	-75.2 (s, 1 F, *endo*) -73.9 (s, 7 F, *exo*) -73.3 (s, 1 F, *endo*) -72.0 (s, 7 F, *exo*);
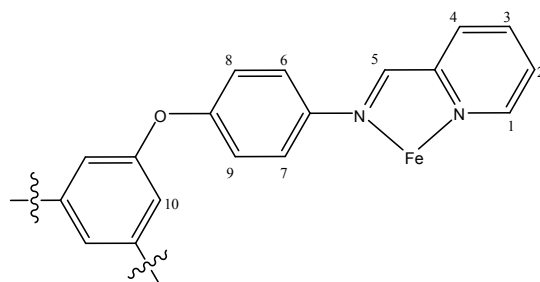
^{1}H NMR data for 2 (significant shifts *cf.* empty cage highlighted: <mark>upfield</mark>, <mark>downfield</mark>)

	$[2](BF_4^-)_8$	$[OTf^-{\subset}2](OTf^-)_7$	$[PF_6^-{\subset}2](PF_6^-)_7$	$[2](ClO_4^-)_8$	$[2](NTf_2^-)_8$
H7	5.33	5.46	5.41	5.32	5.32
H6	5.86	5.60	5.58	5.87	5.87
H10	6.23	6.10	6.07	6.22	6.22
H8	6.85	7.06	7.06	6.84	6.84
H9	7.25	7.45	7.33	7.24	7.24
H4	7.39	7.39	7.40	7.40	7.39
H3	7.78	7.75	7.75	7.77	7.78
H2	8.41	8.39	8.39	8.40	8.41
H1	8.54	8.48	8.48	8.51	8.53
H5	8.94	8.86	8.85	8.94	8.94

^{19}F NMR data for 2

$[2][BF_4^-]$:	-151.1 (*exo*)
$[OTf^-]{\subset}2$:	-79.3 (s, 7 F, *exo*) -78.6 (s, 1F, *endo*)
$[PF_6^-]{\subset}2$:	-76.0 (s, 1 F, *endo*) -74.1 (s, 1 F, *endo*) -73.6 (s, 9 F, *exo*) -71.7 (s, 9 F, *exo*)
$[NTf_2^-]2$:	-80.2 (*exo*)

X-ray structural characterisation

The structural analysis of $\{[BF_4^-\subset1]^{7+}[BF_4^-]_7\}\cdot12MeCN\cdot H_2O$ was carried out on the MX-2 beamline at the Australian synchrotron using synchrotron (λ = 0.71073 Å) radiation. BluIce[S3] was used for the data collection while XDS[S4] was used for data processing. The structure was solved using direct methods with SHELXS[S5] and refined on *Olex2*[S6] using all data by full matrix least-squares procedures with SHELXL.[S7] All of the external BF_4^- anions were restrained (DFIX) to follow the tetrahedral geometry expected for BF_4^- and four (B1, B3, B6, B7) had their thermal parameters constrained to be roughly equal (EDAP). The geometries of 7 of the MeCN molecules were restrained using SAME. All solvent molecules and the BF_4^- ions were refined isotropically. The remaining residual electron density was not modelled and the SQUEEZE[S8] protocol inside PLATON was used to remove the void electron density (total 113 electrons per unit cell). These were included in the molecular weight as 5 MeCN molecules per unit cell (2.5 MeCN per cage).

The structural analysis of $\{[OTf^-\subset1]^{7+}[OTf^-]_7\}\cdot5.63MeCN\cdot3.88H_2O$ and $\{[2]_2^{8+}[NTf^-]_{16}\}\cdot46.17MeCN\cdot$ $\cdot6.5H_2O$ was performed on an Agilent dual wavelength SuperNova with monochromated Cu-*Ka* (l.54178 = Å) radiation. CrysAlisPro[S9] was used for the data collection and data processing. The structure was solved using direct methods with SHELXS[S5] and refined on *Olex2*[S6] using all data by full matrix least-squares procedures with SHELXL.[S7] Multi-scan absorption correction using SCALE3 ABSPACK.[S10] Hydrogen atoms were included in calculated positions with isotropic displacement parameters 1.2 times the isotropic equivalent of their carrier atoms. For $\{[OTf^-\subset1]^{7+}[OTf^-]_7\}\cdot5.63MeCN\cdot3.88H_2O$, all of the external anions and solvent molecules were poorly defined or disordered and have been restrained to show chemically sensible bond lengths and geometries (DFIX and DANG). Five of the OTf^- anions also had their thermal parameters constrained to be roughly equal (EDAP). The internal OTf^- is disordered over three positions with some atoms sharing the same position (EXYZ).All solvent molecules and the OTf^- anions were refined isotropically. The remaining residual electron density was not modelled and the SQUEEZE[S8] protocol inside PLATON was used to remove the void electron density (total of 1048 electrons per unit cell). These were included in the molecular weight as 17 MeCN, 9 H_2O and 8 OTf^- molecules per unit cell (2.125 MeCN, 1.125 H_2O and 1 OTf^- per cage). For $\{[2]_2^{8+}[NTf^-]_{16}\}\cdot46.17MeCN\cdot6.5H_2O$, ten of the anions were poorly defined or disordered and have been restrained to show chemically sensible bond lengths and geometries (DFIX and DANG). Some anions also had their thermal parameters restrained to be roughly equal. These ten anions were refined isotropically while the remaining four anions that could be located were refined anisotropically. One MeCN solvent molecule was disordered and has been restrained to show chemically sensible bond lengths and geometry (DFIX and DANG). Seven of the MeCN solvent molecules were refined isotropically, while the rest were refined anisotropically. The remaining residual electron density was not modelled and the SQUEEZE[S8] protocol inside PLATON was used to remove the void electron density (total of 4304 electrons per unit cell). These were included in the molecular weight as 134 MeCN, 26 H_2O and 8 NTf^- molecules per unit cell (33.5 MeCN, 6.5 H_2O and 2 NTf^- per asymmetric unit).

Table S1. Crystal data for $\{[BF_4^-\subset1]^{7+}[BF_4^-]_7\}\cdot12MeCN\cdot H_2O$, $\{[OTf^-\subset1]^{7+}[OTf^-]_7\}\cdot5.63MeCN\cdot3.88H_2O$ and $[2]^{8+}[NTf^-]_8$

	$\{[BF_4^-\subset1]^{7+}[BF_4^-]_7\}\cdot12MeCN\cdot H_2O$	$\{[OTf^-\subset1]^{7+}[OTf^-]_7\}\cdot5.63MeCN\cdot3.88H_2O$	$\{[2]_2^{8+}[NTf^-]_{16}\}\cdot46.17MeCN\cdot6.5H_2O$
empirical formula	$C_{181}H_{147.5}N_{48.5}O_{13}Fe_4B_8F_{32}$	$C_{175.25}H_{132.63}N_{41.63}O_{39.88}Fe_4S_8F_{24}$	$C_{460.34}H_{391.51}N_{110.17}O_{94.5}Fe_8S_{32}F_{96}$
formula weight	4127.84	4395.53	12275.75
Temperature	100(2) K	120(1) K	120(1) K
Wavelength	0.71073 Å	1.54178 Å	1.54178 Å
crystal system, space group	triclinic, P–1	monoclinic, $C2/c$	monoclinic, $P2_1/c$
Volume	9222(3) Å^3	40936(1) Å^3	52156(1) Å^3
Z	2	8	4
calculated density	1.449 g cm^{-3}	1.426 g cm^{-3}	1.563 g cm^{-3}
absorption coefficient	0.414 mm^{-1}	3.887 mm^{-1}	3.990 mm^{-1}
crystal size	0.11 × 0.06 × 0.03 mm	0.14 × 0.12 × 0.08 mm	0.23 × 0.20 × 0.14 mm
unit cell dimensions	a = 21.800(4) Å α = 103.56(3)°	a = 36.1264(6) Å	a = 44.5214(9) Å
	b = 22.237(4) Å β = 95.35(3)°	b = 39.5634(6) Å β = 99.587(1)°	b = 27.5022(3) Å β = 113.394(2)°
	c = 22.317(5) Å γ = 115.89(3)°	c = 29.0472(4) Å	c = 46.4109(9) Å
$\theta_{\text{min, max}}$	1.07, 23.14	5.55, 65.09	5.55, 65.09
limiting indices	$-23 \leq h \leq 24$, $-24 \leq k \leq 24$, $-24 \leq l \leq 24$	$-40 \leq h \leq 42$, $-46 \leq k \leq 33$, $-34 \leq l \leq 34$	$-46 \leq h \leq 52$, $-32 \leq k \leq 23$, $-54 \leq l \leq 50$
N/N_{ind}	92634/24491 (R_{int} 0.0585)	103300/34781 (R_{int} 0.0465)	186248/88721 (R_{int} 0.0654)
reflns/paramaters/restraints	24491/2145/154	34781/2274/136	88721/5155/243
$T_{\text{min,max}}$	N/A	0.274, 1.000	0.837, 1.000
GoF	1.619	1.310	1.045
final R indices [$I > 2\sigma(I)$]^a	$R_1(F)$ 0.1325, $wR_2(F^2)$ 0.3831	$R_1(F)$ 0.1469, $wR_2(F^2)$ 0.3851	$R_1(F)$ 0.1293, $wR_2(F^2)$ 0.3343
$\Delta\rho_{\text{min,max}}$	-1.30, 1.49 e$^-$Å^{-3}	-1.27, 1.71 e$^-$Å^{-3}	-1.27, 2.16 e$^-$Å^{-3}

^{a} $R_1 = \Sigma(|F_o|-|F_c|)/\Sigma(|F_o|)$; $wR_2 = [\Sigma\{w(F_o^2-F_c^2)^2/\Sigma\{w(F_o^2)^2\}\}]^{1/2}$
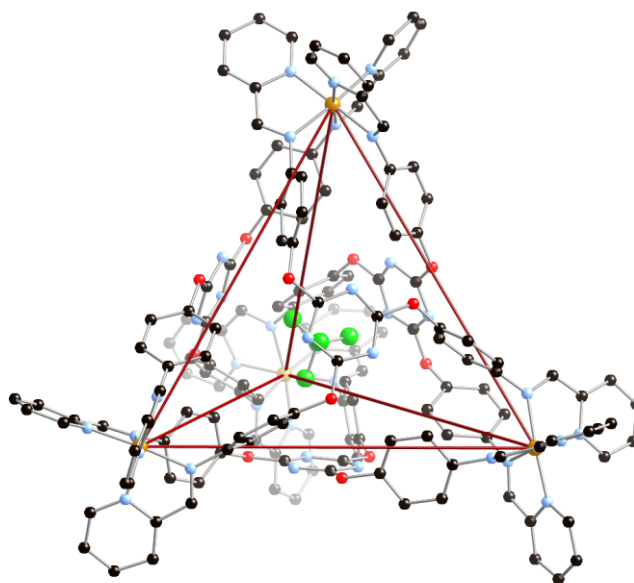
Fig. S1 Crystal structure of $[BF_4^- \subset \mathbf{1}][BF_4^-]_7$ showing the encapsulated BF_4^- anion. Hydrogen atoms, lattice anions and solvent molecules removed for clarity.
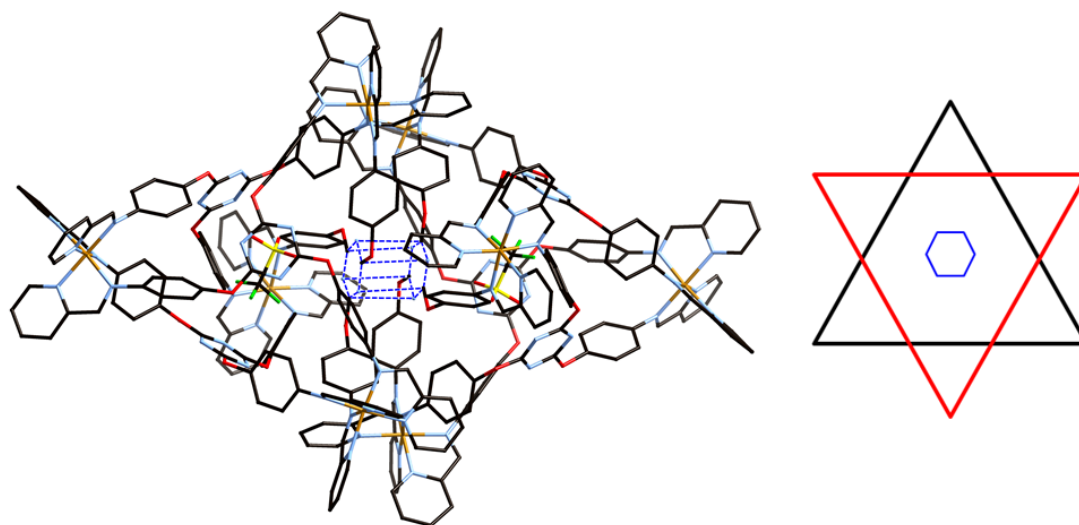
Fig. S2 *Left*: Crystal packing of $[OTf^- \subset \mathbf{1}][OTf^-]_7$, showing the encapsulated OTf^- anion and the face-to-face π- π interactions (blue dashed lines) between neighbouring molecules. *Right*: representation of the offset nature of the metal centres (points of the triangle) in the face-to-face packing interaction. Hydrogen atoms, lattice anions and solvent molecules removed for clarity.
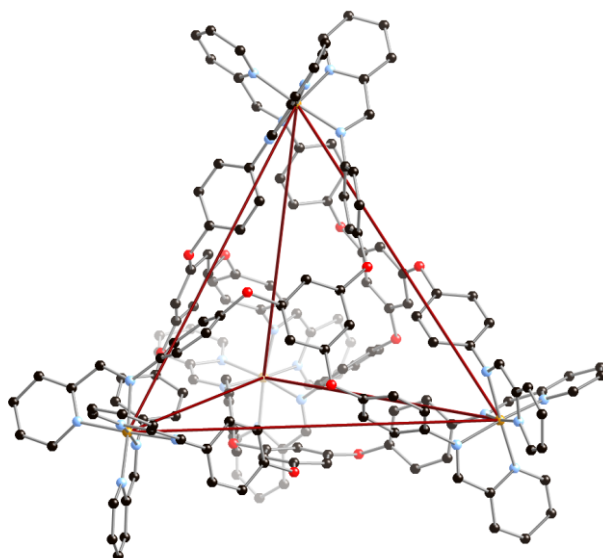
Fig. S3 Crystal structure of [**2**][NTf$_2^-$]$_8$ showing the empty cage. Hydrogen atoms, anions and solvent molecules removed for clarity.

Exchange studies for 1

General procedure for exchange studies: A CD_3CN solution (500 µL) of [guest⊂**1**] of known concentration was added to an NMR tube and the ^{19}F NMR spectrum was collected. To this NMR tube was added 1 equivalent (with respect to the anion present) of the TBA salt of the competing anion. The ^{19}F NMR spectrum was collected without heating, showing no exchange had taken place. The tube was then heated at 50 °C overnight and once again the ^{19}F NMR spectrum collected. Heating was repeated until complete exchange was achieved or equilibrium had been reached.
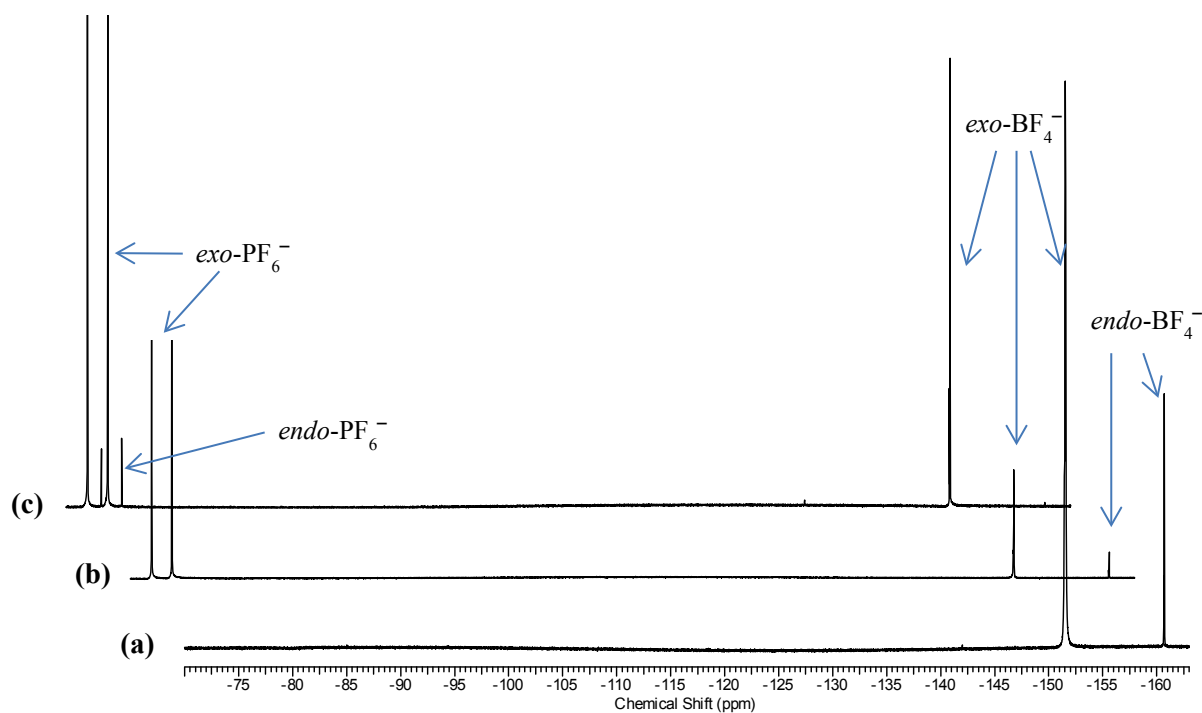
Fig. S4 ^{19}F NMR stack plot showing the conversion of [BF_4^-⊂**1**] to [PF_6^-⊂**1**]. **(a)** [BF_4^-⊂**1**] showing resonances for both *endo-* and *exo-*BF_4^-. **(b)** After addition of [TBA·PF_6] showing resonances for both *endo-* and *exo-*BF_4^- in addition to *exo-*PF_6^- (no exchange). **(c)** After heating the solution from **(b)** at 50 °C overnight showing resonances for *exo-*BF_4^- (only) in addition to *exo-*PF_6^- (small) and *endo-*PF_6^- (full exchange). (CD_3CN, 376 MHz, 298 K).
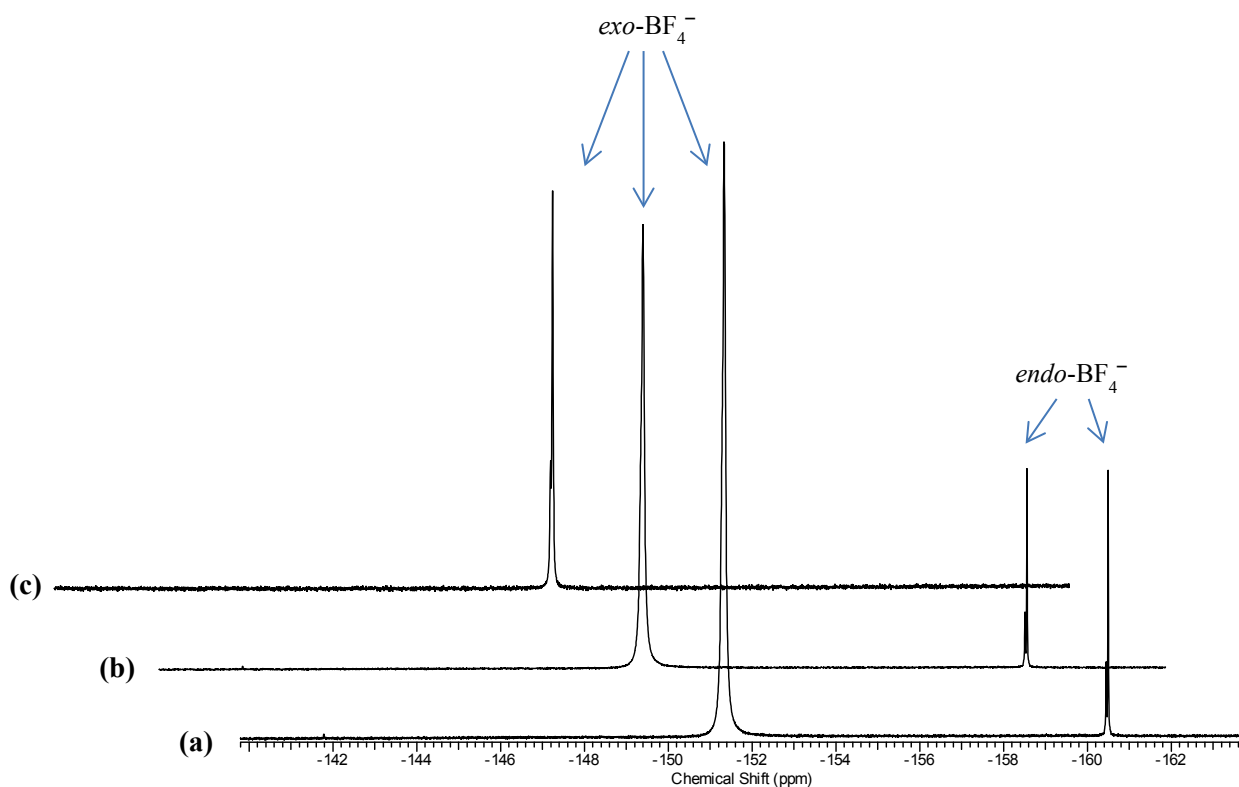
Fig. S5 ^{19}F NMR stack plot showing the conversion of [BF$_4^-$⊂**1**] to [ClO$_4^-$⊂**1**]. **(a)** [BF$_4^-$⊂**1**] showing resonances for both *endo-* and *exo-*BF$_4^-$. **(b)** After addition of [TBA·ClO$_4$] showing resonances for both *endo-* and *exo-*BF$_4^-$ (no exchange). **(c)** After heating the solution from **(b)** at 50 °C overnight showing resonances for only *exo-*BF$_4^-$ (full exchange). (CD$_3$CN, 376 MHz, 298 K).
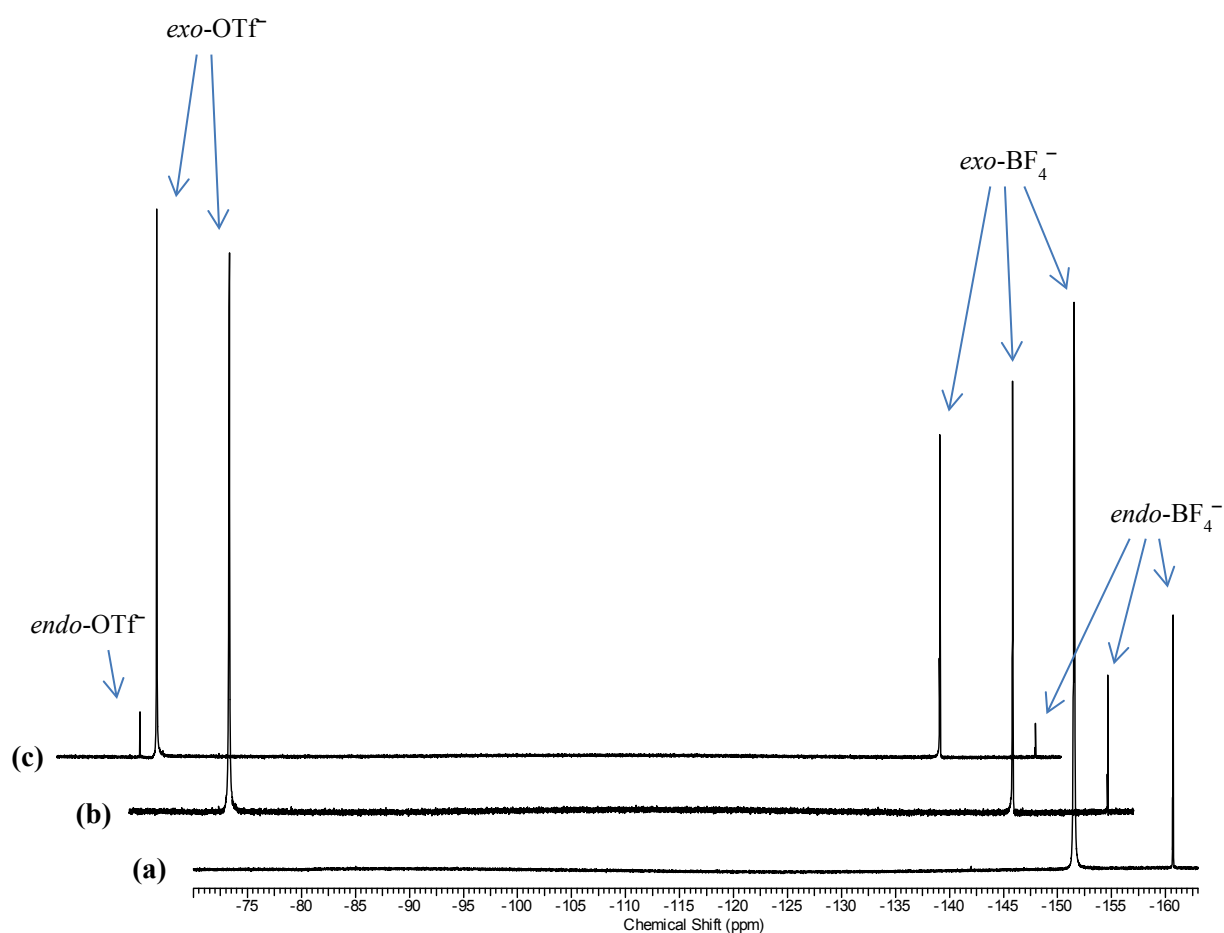
Fig. S5 ^{19}F NMR stack plot showing the incomplete conversion of [BF$_4^-$⊂**1**] to [OTf$^-$⊂**1**]. **(a)** [BF$_4^-$⊂**1**] showing resonances for both *endo-* and *exo*-BF$_4^-$. **(b)** After addition of [TBA·OTf] showing resonances for both *endo-* and *exo*-BF$_4^-$ in addition to *exo*-OTf$^-$ (no exchange). **(c)** After heating the solution from **(b)** at 50 °C overnight showing resonances for *exo*-BF$_4^-$ and *endo*-BF$_4^-$ in addition to *exo*-OTf$^-$ and *endo*-OTf$^-$ (incomplete exchange). (CD$_3$CN, 376 MHz, 298 K).
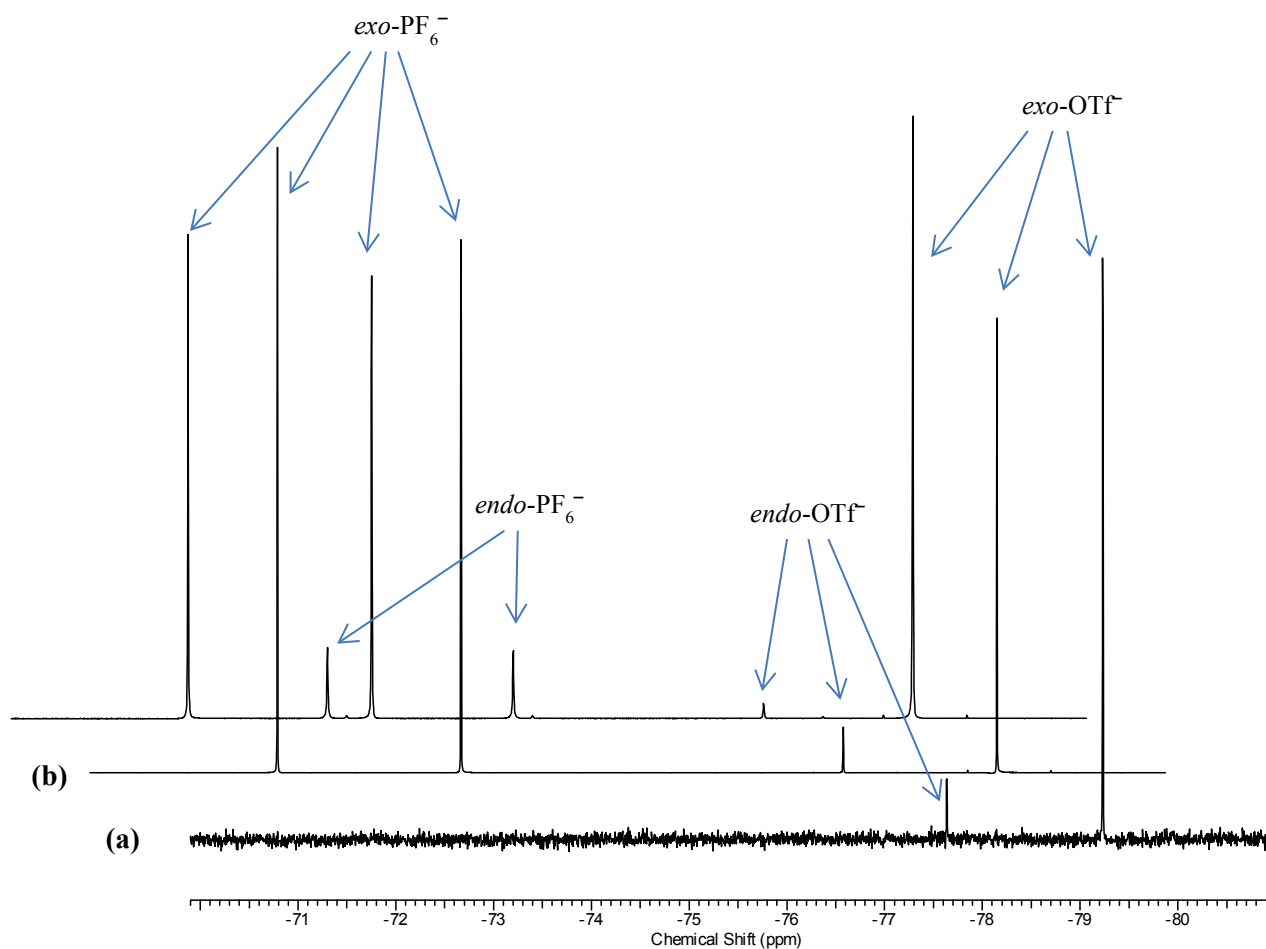
Fig. S6 ^{19}F NMR stack plot showing the incomplete conversion of [OTf⁻⊂**1**] to [PF$_6$⁻⊂**1**]. **(a)** [OTf⁻⊂**1**] showing resonances for both *endo-* and *exo*-OTf⁻. **(b)** After addition of [TBA·PF$_6$] showing resonances for both *endo-* and *exo*-OTf⁻ in addition to *exo*-PF$_6$⁻ (no exchange). **(c)** After heating the solution from **(b)** at 50 °C for 72 hrs showing resonances for *exo*-OTf⁻ and *endo*-OTf⁻ in addition to *exo*-PF$_6$⁻ and *endo*-PF$_6$⁻ (incomplete exchange). (CD$_3$CN, 376 MHz, 298 K).

Competitive formation studies of 1

General procedure for competition experiments: 25 mg of 2,4,6-tris(4-aminophenoxy)triazine (0.063 mmol) was dissolved in 10 mL of CH_3CN. To this solution 1.80 mL (0.189 mmol) of a 2-pyridinecarboxaldehyde-MeCN stock solution (1:100) was added with stirring. A 50:50 mixture of two solid $Fe(A^-)_2$ salts (0.063 mmol based on Fe) ($A^- = BF_4^-$; OTf^-; PF_6^-; or ClO_4^-) were combined in CH_3CN (5 mL) and added to the ligand sub-component solution producing deep purple solutions, which were heated at ~50 °C overnight. ^1H and ^{19}F NMR samples were prepared by taking small portions of the reaction mixtures, removing the solvent, and then dissolving the residues in CD_3CN.

BF_4^- vs. PF_6^-.
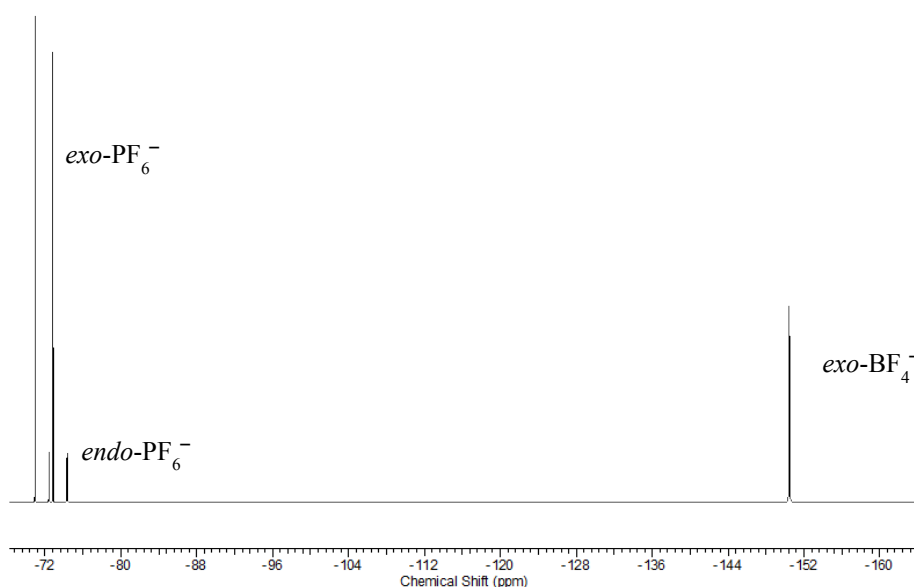
Fig. S7 ^{19}F NMR spectrum showing the exclusive formation of $[PF_6^- \subset \mathbf{1}]$ in preference to $[BF_4^- \subset \mathbf{1}]$ during the competitive formation experiment between $Fe(A^-)_2$ salts where A^- is either BF_4^- or PF_6^-. (CD_3CN, 376 MHz, 298 K).

BF_4^- vs. OTf^-.
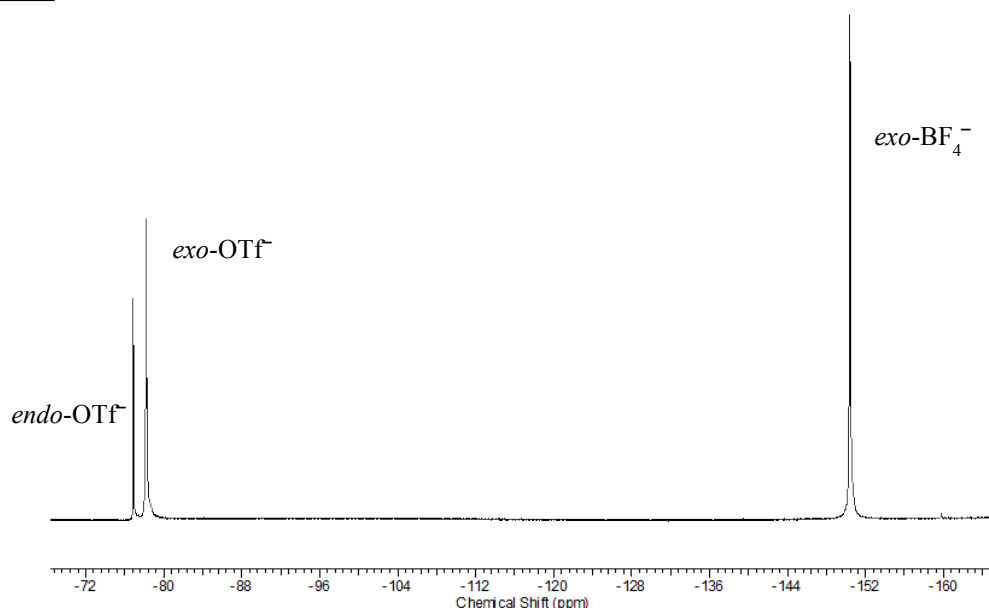
Fig. S8 ^{19}F NMR spectrum showing the exclusive formation of $[OTf^- \subset \mathbf{1}]$ in preference to $[BF_4^- \subset \mathbf{1}]$ during the competitive formation experiment between $Fe(A^-)_2$ salts where A^- is either BF_4^- or OTf^-. (CD_3CN, 376 MHz, 298 K).

PF$_6^-$ *vs.* OTf$^-$
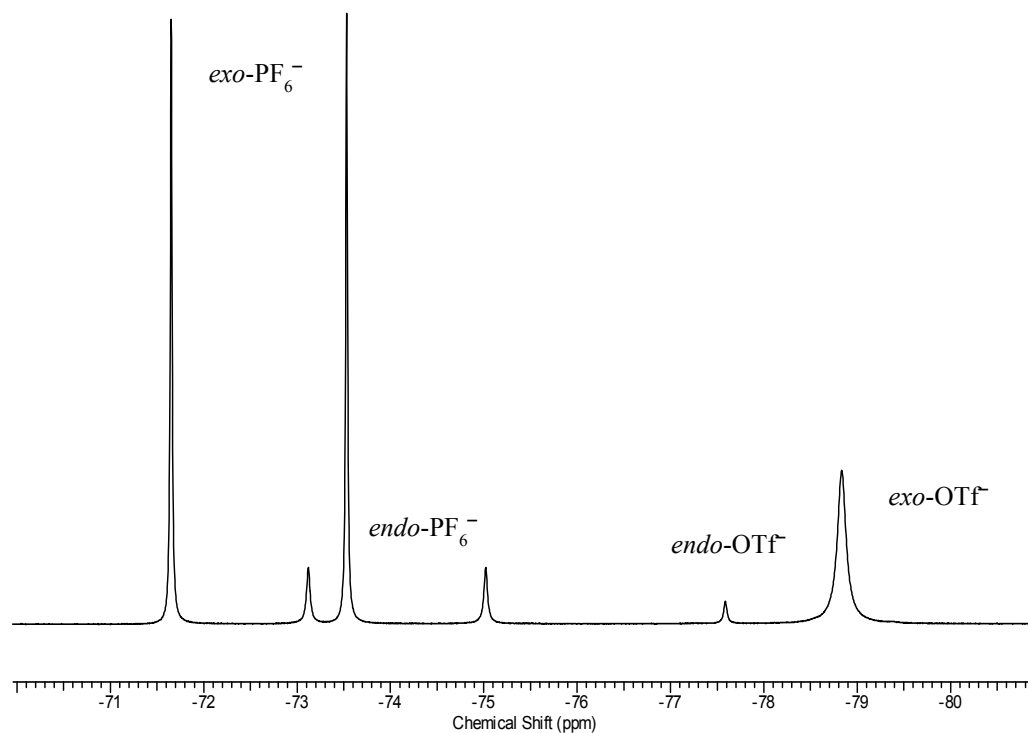
Fig. S9 ^{19}F NMR spectrum showing the formation of both [PF$_6^-$⊂**1**] and [OTf$^-$⊂**1**] during the competitive formation experiment between Fe(A$^-$)$_2$ salts where A$^-$ is either PF$_6^-$ or OTf$^-$. (CD$_3$CN, 376 MHz, 298 K).

ClO$_4^-$ *vs.* PF$_6^-$
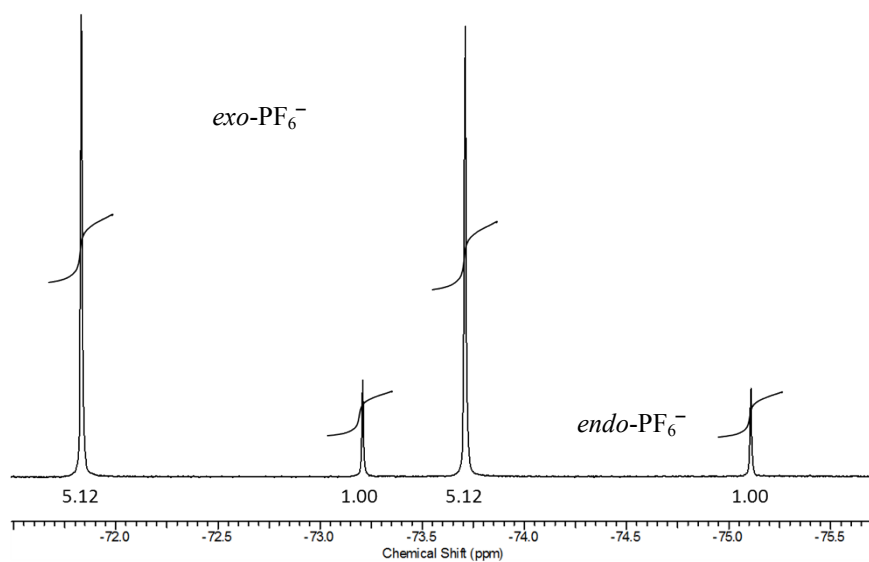
Fig. S10 ^{19}F NMR spectrum showing the formation of both [PF$_6^-$⊂**1**] and [ClO$_4^-$⊂**1**] during the competitive formation experiment between Fe(A$^-$)$_2$ salts where A$^-$ is either PF$_6^-$ or ClO$_4^-$. The spectrum suggests a mixture of [PF$_6^-$⊂**1**] and [ClO$_4^-$⊂**1**] has formed. If only PF$_6^-$ was encapsulated the ratio of *endo-* to *exo-* PF$_6^-$ would be 1:3. Here it is 1:5, suggesting a mixture of [PF$_6^-$⊂**1**] and [ClO$_4^-$⊂**1**] in 3:2 ratio. (CD$_3$CN, 376 MHz, 298 K).

ClO$_4^-$ *vs.* OTf$^-$
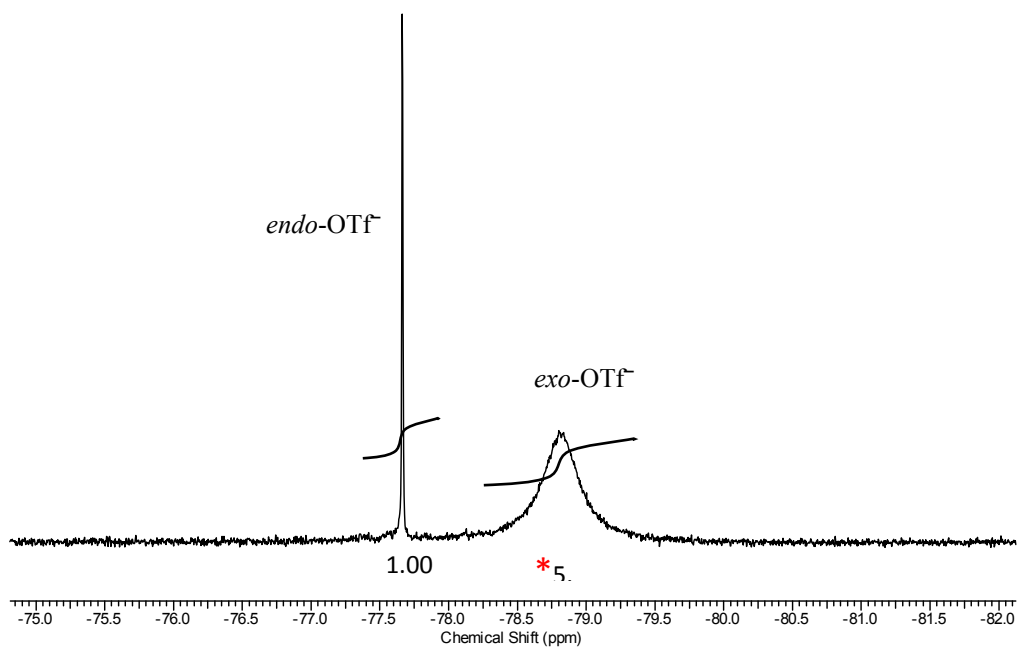
Fig. S11 ^{19}F NMR spectrum showing the formation of both [ClO$_4^-$⊂**1**] and [OTf$^-$⊂**1**] during the competitive formation experiment between Fe(A$^-$)$_2$ salts where A$^-$ is either ClO$_4^-$ or OTf$^-$. The spectrum suggests a mixture of [PF$_6^-$⊂**1**] and [ClO$_4^-$⊂**1**] has formed. If only OTf$^-$ was encapsulated the ratio of *endo*- to *exo*-OTf$^-$ would be 1:3. Here it is 1:5, suggesting a mixture of [OTf$^-$⊂**1**] and [ClO$_4^-$⊂**1**] in 3:2 ratio. (CD$_3$CN, 376 MHz, 298 K).

Anion binding studies for 2

General procedure for binding studies of suitable guests: A stock solution (CD$_3$CN) of empty **2** ($\times 10^{-4}$ M) was prepared. 500 µL of this solution was transferred to an NMR tube and then 5 µL aliquots of a CH$_3$CN solution of the appropriate TBA$^+$.A$^-$ salt were added sequentially until complete formation of [guest⊂**2**] or equilibrium had been reached.
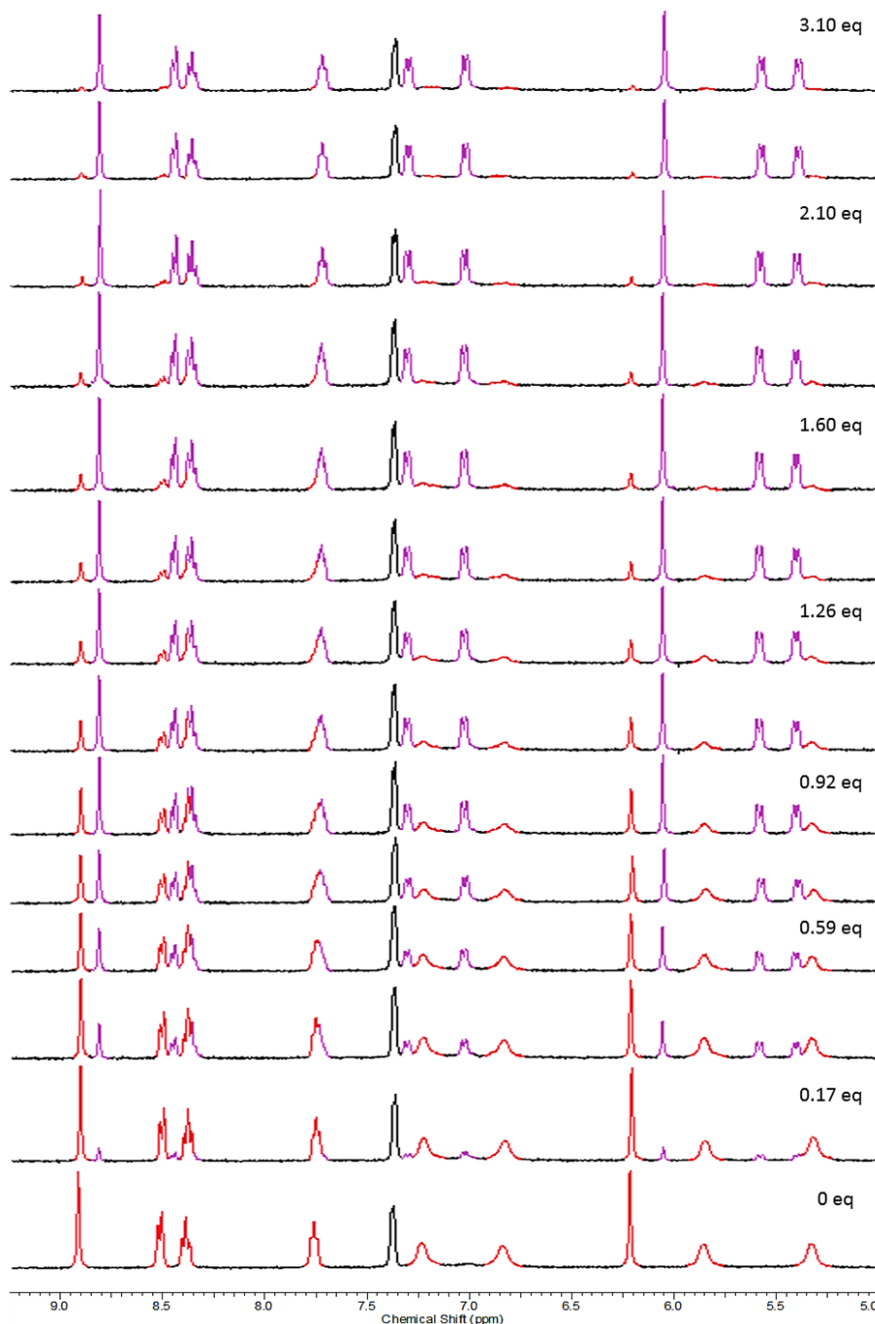
Fig. S12 Partial ^{1}H NMR spectra for the titration of 'guest-free' cage [**2**]$^{8+}$ (bottom) with TBA$^+$.PF$_6^-$ to give [PF$_6^-$⊂**2**]$^{7+}$ (above). (CD$_3$CN, 400 MHz, 298 K).
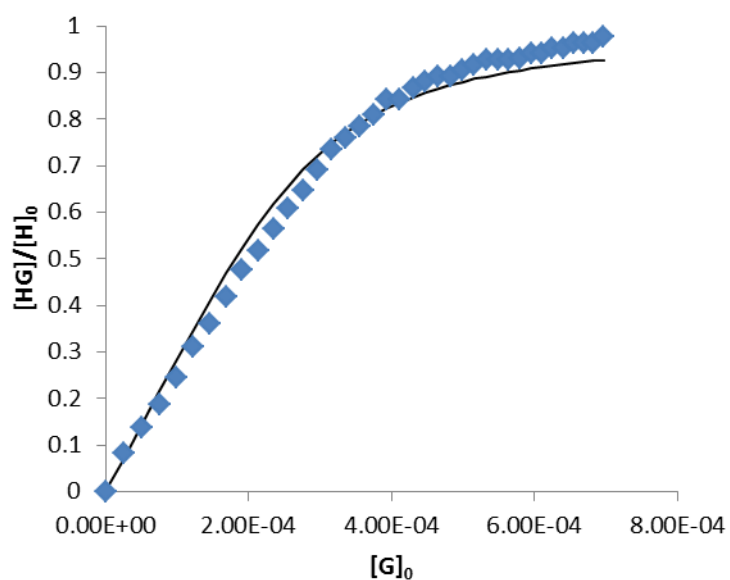
Fig. S13 Fitting of the data for the titration of $TBA^+.PF_6^-$ into empty **2**, $K_a = 2.61 \times 10^4 \pm 1.6 \times 10^3$ M^{-1}.
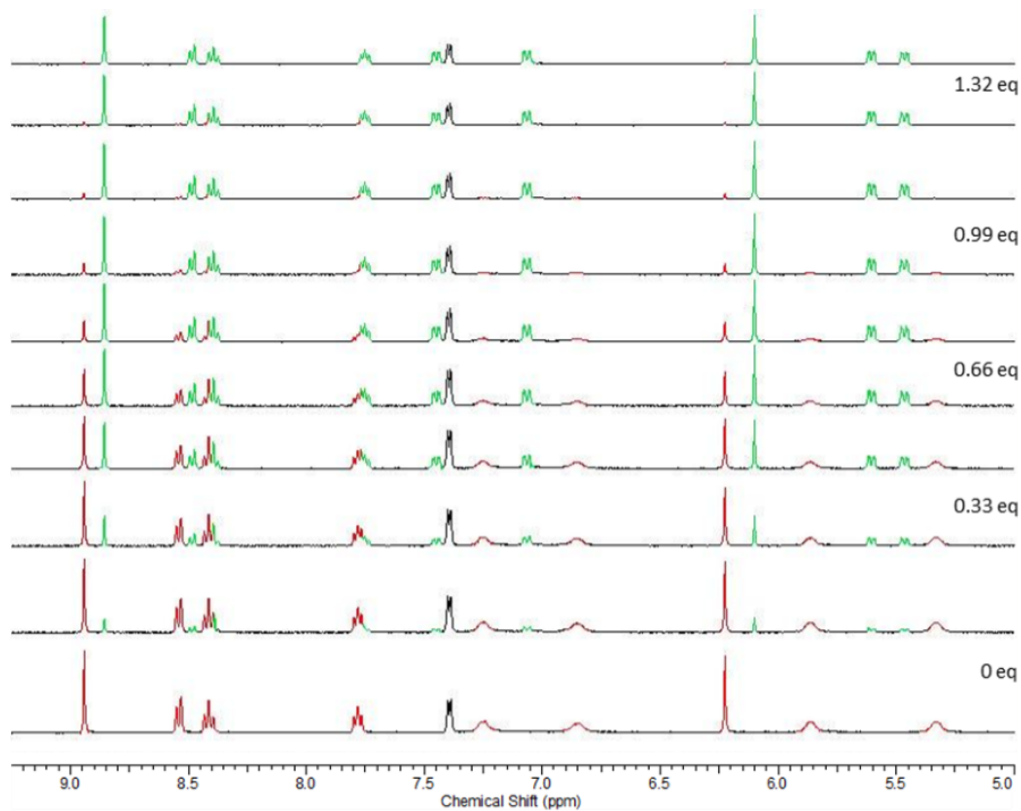
Fig. S14 Partial ^1H NMR spectra for the titration of 'guest-free' cage $[2]^{8+}$ (bottom) with $TBA^+.OTf^-$ to give $[OTf^- \subset 2]^{7+}$ (above). (CD_3CN, 400 MHz, 298 K).
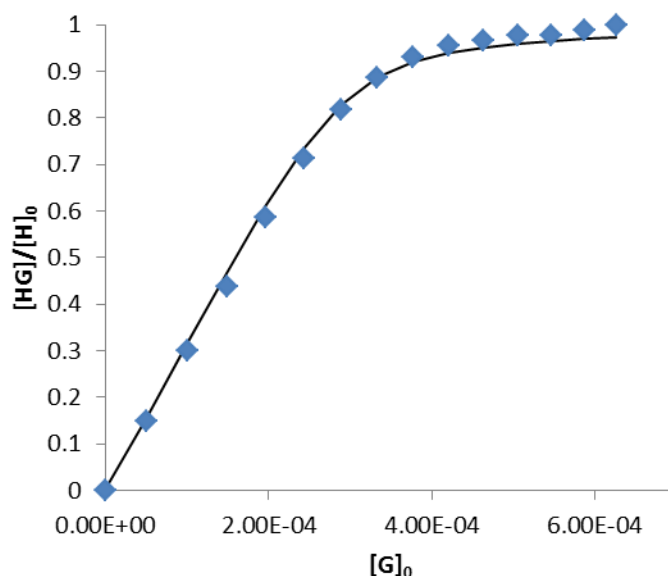
Fig. S15 Fitting of the data for the titration of TBA$^+$.OTf$^-$ into empty **2**, $K_a = 9.9 \times 10^4 \pm 1.0 \times 10^4$ M^{-1}.

Determination of binding constants for 2 for data in Fig. S13 and Fig. S15

Set: $\quad a = \dfrac{1}{2K[H]0} \qquad\qquad B = 1 + K([H]_0 + [G]_0) \qquad\qquad c = 4K^2[H]_0[G]_0 \qquad\qquad f = (b^2 - c)^{1/2}$

then according to Hristova *et al.*[S11]

$y_{calc} = a(b^2 - f)$

The first derivatives are:

$$\dfrac{da}{dK} = \dfrac{-a}{K} \qquad\qquad \dfrac{db}{dK} = \textbf{Error!} \qquad\qquad \dfrac{dc}{dK} = \dfrac{2c}{K} \qquad\qquad \dfrac{df}{dK} = \textbf{Error!}$$

$$\dfrac{dycalc}{dK} = \dfrac{a}{K}$$

To get the uncertainty, define:

$S = \textbf{Error!} \qquad\qquad W =$

Where *n* is the number of data. The estimated standard deviation of K is:

$s_K = \qquad {}^{1/2}$
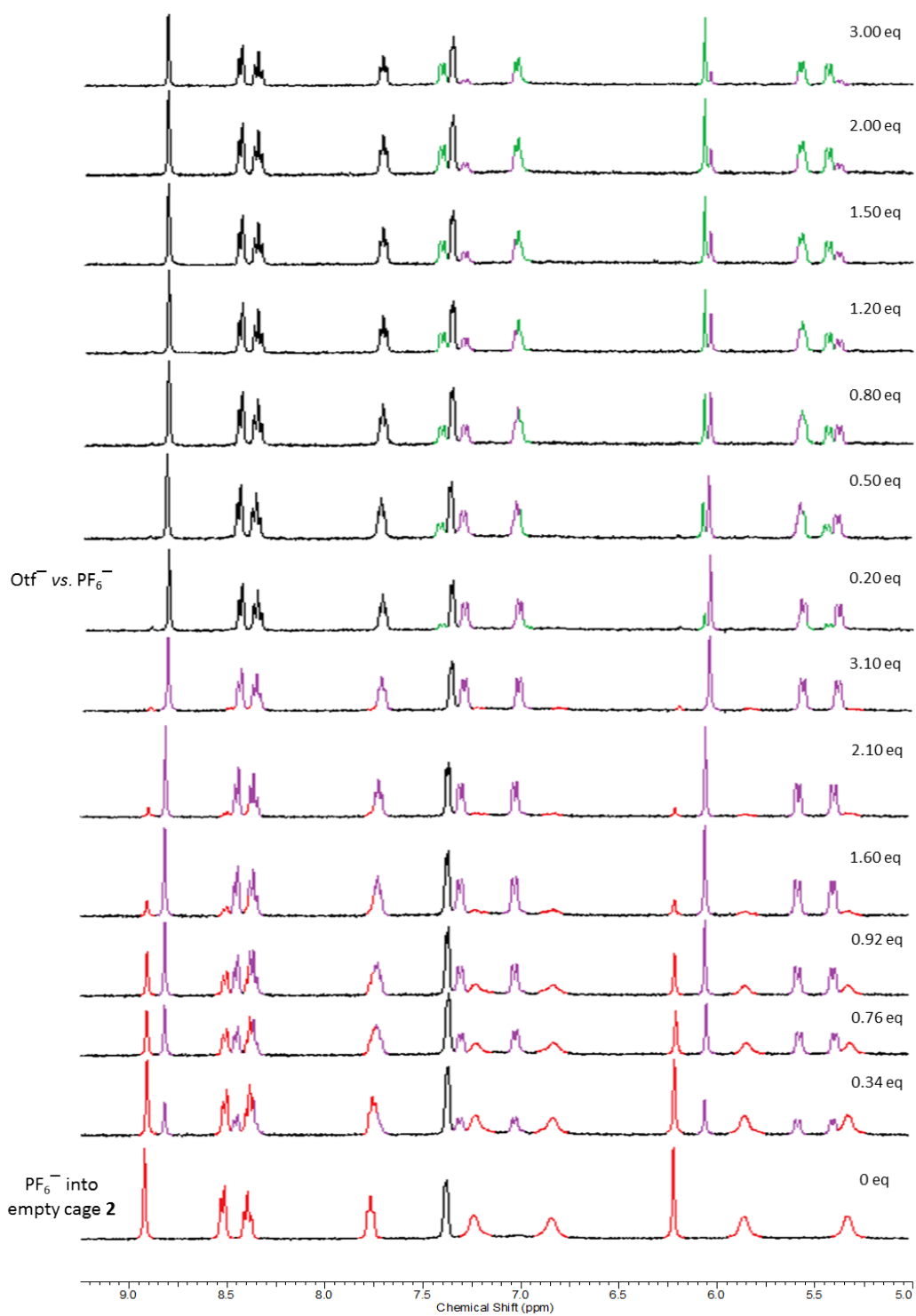
Fig. S16 Partial ^{1}H NMR spectra for the titration of 'guest-free' cage [**2**]$^{8+}$ with TBA$^+$·PF$_6{}^-$ to first form [PF$_6{}^-$⊂**2**]$^{7+}$ followed by the sequential addition of TBA$^+$.Otf$^-$ to displace PF$_6{}^-$ to then give [Otf$^-$⊂**2**]$^{7+}$ (top). (CD$_3$CN, 400 MHz, 298 K).
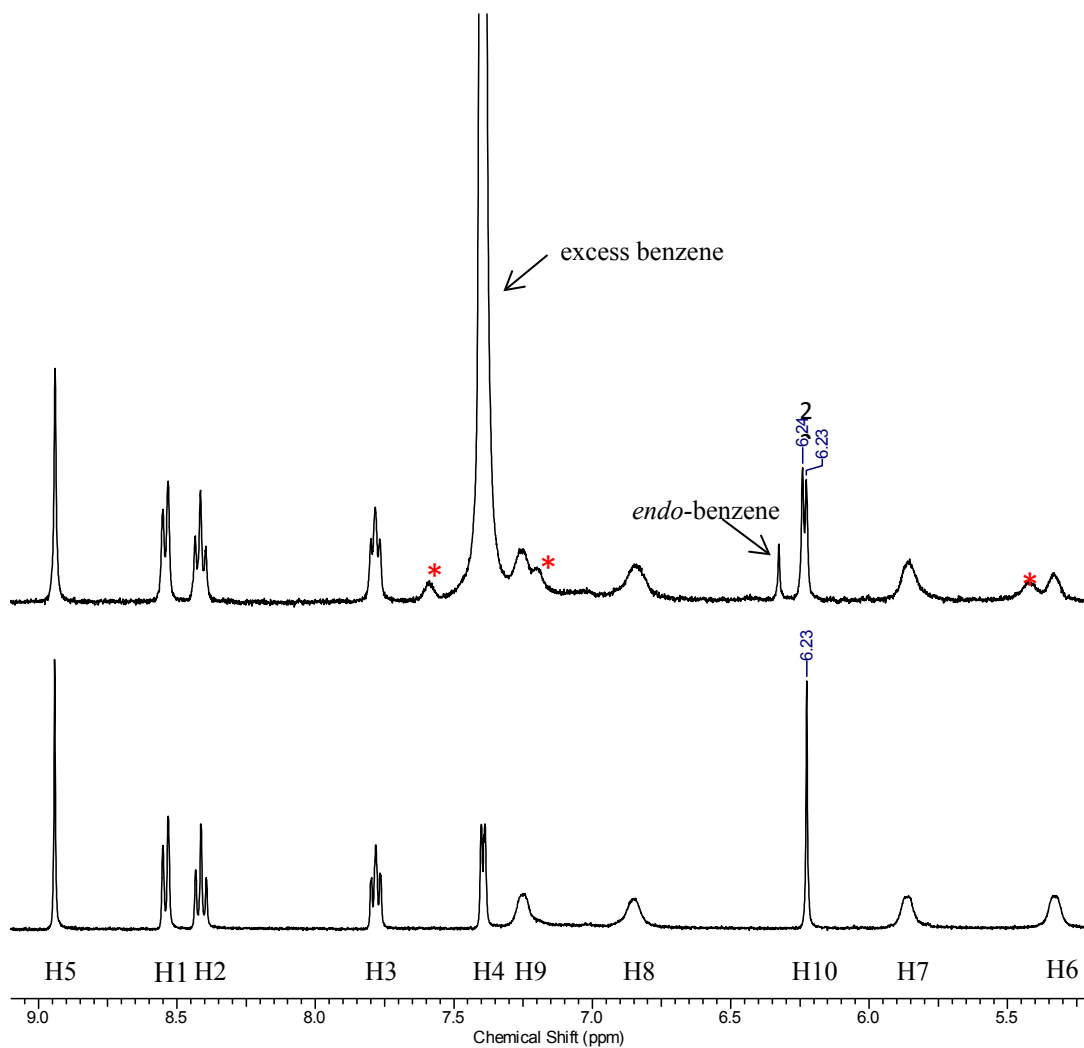
Fig. S17 *Top*: ^{1}H NMR spectrum after addition of excess benzene into empty cage **2**. Peaks attributed to [benzene⊂**2**] highlighted with red star. *Bottom*: ^{1}H NMR spectrum of empty cage **2**. (CD$_3$CN, 400 MHz, 298 K).

Table S2: Guests explored and their van der Waals volumes (Å^3)

Guest	Volume (Å^3)	Encapsulation observed?	
		Cage 1	Cage 2
PF$_6^-$	75	Yes	Yes
OTf$^-$	86	Yes	Yes
ClO$_4^-$	55	Yes	No
BF$_4^-$	59	Yes	No
NTf$_2^-$	157	No	No
Benzene	99	No	Yes
CHCl$_3$	75	No	No
CCl$_4$	89	No	No

References

S1.   F.C. Schaefer, J.T. Thurston and J.R. Dudley, *J. Am. Chem. Soc.*, 1951, **73**, 2990; A. Ferguson, M. A. Squire, D. Siretanu, D. Mitcov, C. Mathonière, R. Clérac and P.E. Kruger, *Chem. Commun.*, 2013, **49**, 1597.

S2.   M. Yamanaka and H. Fujii, *J. Org. Chem.*, 2009, **74**, 5390.

S3.   T.M. McPhillips, S.E. McPhillips, H.J. Chiu, A.E. Cohen, A.M. Deacon, P.J. Ellis, E. Garman, A. Gonzalez, N.K. Sauter, R.P. Phizackerley, S.M. Soltis and P. Kuhn, *J. Synchrotron Radiat.*, 2002, **9**, 401.

S4.   W. Kabsch, *J. Appl. Cryst.*, 1993, **26**, 795.

S5.   G.M. Sheldrick, *Acta Cryst., Sect. A: Fundam. Crystallogr.*, 1990, **46**, 467.

S6.   O.V. Dolomanov, L.J. Bourhis, R.J. Gildea, J.A.K. Howard and H. Puschmann, *J. Appl. Cryst.*, 2009, **42**, 339.

S7.   G.M. Sheldrick, *Acta Cryst.*, 2008, **A64**, 112.

S8.   A.L. Spek, *PLATON, A Multipurpose Crystallographic Tool*, Utrecht University, Utrecht, The Netherlands, 2008.

S9.   CrysAlisPro, Agilent Technologies, Version 1.171.35.19.

S10.   CrysAlisPro, Agilent Technologies, Version 1.171.35.19; Empirical absorption correction using spherical harmonics, implemented in SCALE3 ABSPACK scaling algorithm.

S11.   Y.R. Hristova, M.M.J. Smulders, J.K. Clegg, B. Breiner and J.R. Nitschke, *Chem. Sci.*, 2011, **2**, 638